SCIENCE CHINA
Information Sciences

• RESEARCH PAPER •

February 2022, Vol. 65 122409:1–122409:7
https://doi.org/10.1007/s11432-021-3297-x

Analyzing electrostatic modulation of signal transduction efficiency in MoS_2 nanoelectromechanical resonators with interferometric readout

Jiankai ZHU[1†], Pengcheng ZHANG[2†], Rui YANG[2*] & Zenghui WANG[1*]

[1]*Institute of Fundamental and Frontier Sciences, University of Electronic Science and Technology of China, Chengdu* 610054*, China;*
[2]*University of Michigan-Shanghai Jiao Tong University Joint Institute, Shanghai Jiao Tong University, Shanghai* 200240*, China*

Received 22 April 2021/Revised 6 June 2021/Accepted 23 July 2021/Published online 14 January 2022

Abstract Optical interferometry is a highly sensitive method for detecting the miniscule resonant motion in two-dimensional (2D) nanoelectromechanical systems (NEMS). However, the technique to control the interferometry signal strength has not been fully understood. In this work, we present analytical modeling of an effective method for tuning motion-to-signal responsivity in interferometric detection of 2D molybdenum disulfide (MoS_2) NEMS resonators. We show that the responsivity can be tuned very efficiently, all the way from maximum to 0, by varying the vacuum gap underneath the 2D membrane electrostatically. We further show that the gate voltage corresponding to 0 responsivity, which means no motion signal can be detected, varies with the MoS_2 thickness, diameter, pre-strain, and initial vacuum gap. Our findings provide an important guideline for optimizing measurement conditions when detecting motion in 2D NEMS structures using laser interferometry.

Keywords MoS_2, 2D NEMS, resonators, laser interferometry, responsivity

Citation Zhu J K, Zhang P C, Yang R, et al. Analyzing electrostatic modulation of signal transduction efficiency in MoS_2 nanoelectromechanical resonators with interferometric readout. Sci China Inf Sci, 2022, 65(2): 122409, https://doi.org/10.1007/s11432-021-3297-x

1 Introduction

Nanoelectromechanical systems (NEMS) based on two-dimensional (2D) materials are promising for designing and realizing novel sensing devices, by combining the mechanical degree of freedom available in such device structures and unique physical properties offered by 2D materials [1–6]. A key challenge for 2D NEMS research is to detect the small mechanical motion in these atomically-thin structures. Since the very first graphene resonator detected by laser interferometry [7], many electrical and optical techniques have been used to detect the motion of 2D NEMS resonators. Electrical detection techniques have good compatibility with on-chip and large-scale integration, with amplitude modulation (AM) mixing [8–10], frequency modulation (FM) mixing [9,11–13], and direct radio-frequency signal transduction schemes [14, 15] explored and implemented in 2D NEMS studies. Optical interferometry motion detection can have very high signal transduction efficiency, i.e., responsivity (signal change per unit device motion). This technique is capable of detecting the thermomechanical resonance induced by the Brownian motion, showing high sensitivity of the measurement system, and can map the mode shapes of the different resonant modes [16–19]. In addition, laser interferometry has been used for studying photothermal back-action and laser cooling in 2D NEMS resonators [20], measuring 2D NEMS suspended on flexible substrates [21], measuring thermal transport in 2D materials [22], and detecting the motion of 2D bimorph

* Corresponding author (email: rui.yang@sjtu.edu.cn, zenghui.wang@uestc.edu.cn)
† Zhu J K and Zhang P C have the same contribution to this work.

resonators [23]. While the dependence of responsivity on 2D device structure has been theoretically studied [24, 25], the opportunity of responsivity tuning by continuously varying the device structures in a controlled manner has remained to be exploited.

Here, we analyze the electrical control of motion-to-signal responsivity in molybdenum disulfide (MoS_2) NEMS resonators. For a suspended 2D membrane with a back gate, the gate voltage can pull down the membrane electrostatically. Such effect can result in an effective tuning of resonance frequency due to the gate-induced strain [8, 15, 18], and is important in the electrical signal transduction in 2D NEMS resonators [26, 27]. By combining electrostatic effect with optical interferometry in our analysis, we show that gate voltage can be used to effectively tune the vacuum gap depth underneath the 2D material, and thus modulate the interferometric responsivity, all the way down to 0 at certain gate voltages. We also analyze responsivity tuning effect by varying device parameters, including MoS_2 thickness, device diameter, pre-strain and initial vacuum gap d_0 (vacuum gap at 0 gate voltage). Since gate voltage is widely used for tuning the conductance and resonance frequency in 2D NEMS devices, our analysis can provide an important reference for optical interferometry detection when coupled with gate tuning.

2 Results

The MoS_2 device used in this analysis takes the form of a circular drumhead (side view shown in Figure 1(a)). The thickness of the suspended MoS_2 is d_1, and the vacuum gap depth is d_2. When the laser beam is incident on the MoS_2 membrane, it is reflected at multiple interfaces: the vacuum-MoS_2 interface, the MoS_2-vacuum interface, and the vacuum-Si interface. The total reflectance, defined by the reflected light intensity divided by the incident light intensity, can be calculated using equations from thin-film optics [17], and can be written as follows:

$$R_{\mathrm{ef}}(r,\theta)=\frac{I_{\mathrm{interferometry}}}{I_{\mathrm{incident}}}=\left|\frac{\boldsymbol{r}_1\mathrm{e}^{\mathrm{i}(\boldsymbol{\varphi}_1+\varphi_2)}+\boldsymbol{r}_2\mathrm{e}^{-\mathrm{i}(\boldsymbol{\varphi}_1-\varphi_2)}+\boldsymbol{r}_3\mathrm{e}^{-\mathrm{i}(\boldsymbol{\varphi}_1+\varphi_2)}+\boldsymbol{r}_1\boldsymbol{r}_2\boldsymbol{r}_3\mathrm{e}^{\mathrm{i}(\boldsymbol{\varphi}_1-\varphi_2)}}{\mathrm{e}^{\mathrm{i}(\boldsymbol{\varphi}_1+\varphi_2)}+\boldsymbol{r}_1\boldsymbol{r}_2\mathrm{e}^{-\mathrm{i}(\boldsymbol{\varphi}_1-\varphi_2)}+\boldsymbol{r}_1\boldsymbol{r}_3\mathrm{e}^{-\mathrm{i}(\boldsymbol{\varphi}_1+\varphi_2)}+\boldsymbol{r}_2\boldsymbol{r}_3\mathrm{e}^{\mathrm{i}(\boldsymbol{\varphi}_1-\varphi_2)}}\right|^2, \quad (1)$$

where $\boldsymbol{r}_1$, $\boldsymbol{r}_2$, and $\boldsymbol{r}_3$ are reflection coefficients at the vacuum-MoS_2, MoS_2-vacuum, and vacuum-Si interface, respectively:

$$\boldsymbol{r}_1=\frac{n_{\mathrm{vac}}-\boldsymbol{n}_{\mathrm{MoS_2}}}{n_{\mathrm{vac}}+\boldsymbol{n}_{\mathrm{MoS_2}}},\quad \boldsymbol{r}_2=\frac{\boldsymbol{n}_{\mathrm{MoS_2}}-n_{\mathrm{vac}}}{\boldsymbol{n}_{\mathrm{MoS_2}}+n_{\mathrm{vac}}},\quad \boldsymbol{r}_3=\frac{n_{\mathrm{vac}}-\boldsymbol{n}_{\mathrm{Si}}}{n_{\mathrm{vac}}+\boldsymbol{n}_{\mathrm{Si}}}, \quad (2)$$

and $\boldsymbol{\varphi}_1$, φ_2 are the phase shifts when the light is traveling in different media:

$$\boldsymbol{\varphi}_1=\frac{2\pi\boldsymbol{n}_{\mathrm{MoS_2}}d_1}{\lambda},\quad \varphi_2=\frac{2\pi n_{\mathrm{vac}}d_2}{\lambda}, \quad (3)$$

where λ is the laser wavelength; here we use 632.8 nm for He-Ne laser, which is commonly used for MEMS/NEMS resonator measurements. In the above equations, each d stands for the thickness, and each $\boldsymbol{n}$ stands for the complex index of refraction of the respective layers (MoS_2, vacuum gap, and silicon), with n_{vac} being the only one with real value, which equals unity. Here we assume the normal incidence of the light. In actual measurements, the light may have a small oblique angle due to imperfection in the optical alignment. Such angle is typically very small (on the order of 0.1°), which results in a negligible effect on the responsivity. The laser spot size is often notably smaller than the device size [17], and for simplicity, we treat it as a point in our analysis, which is a good approximation for most measurement conditions.

As the 2D membrane vibrates, the periodic change in d_2 dynamically modulates the interferometric condition and thus the total reflectance of the device structure (Figure 1(b)). The slope of the curve in Figure 1(b) gives the displacement-to-reflectance responsivity (Figure 1(c)), defined as $\partial R_{\mathrm{ef}}/\partial d_2$. Interestingly, from the analysis of a typical MoS_2 device (Figure 1(b) and (c)), we observe the striking feature that at a specific d_2 value, the reflectance does not change with vacuum gap, which means 0 responsivity for interferometric motion detection—the vibration just cannot be detected using laser interferometry. We denote the d_2 value when such condition is met as $d_{2(0)}$.

When a DC gate voltage V_g is applied between the MoS_2 membrane and the gate electrode underneath, the 2D structure is electrostatically attracted towards the gate, reducing the vacuum gap depth d_2 (Figure 2(a)). Such variation in device structure statically tunes the interferometric condition, and thus

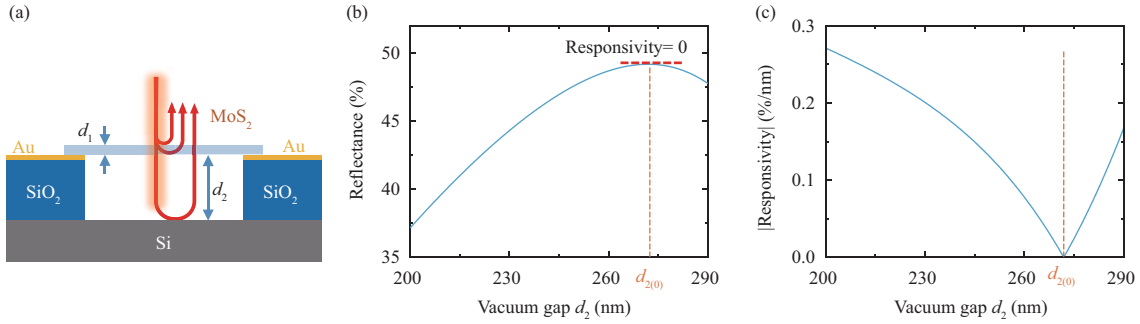

Figure 1 (Color online) Responsivity of laser interferometric motion detection in 2D MoS_2 NEMS resonators. (a) Schematic illustration of the laser interferometry. (b) Calculated reflectance as a function of vacuum gaps d_2, for an MoS_2 device with thickness d_1 of 5 layers (3.25 nm), radius R of 3 μm, initial vacuum gap of 290 nm, pre-strain ε_0 of 0.01%. The result shows how the responsivity is derived using the slope of the curve, and 0 responsivity can be obtained at a specific vacuum gap depth $d_{2(0)}$. (c) Magnitude of responsivity as a function d_2.

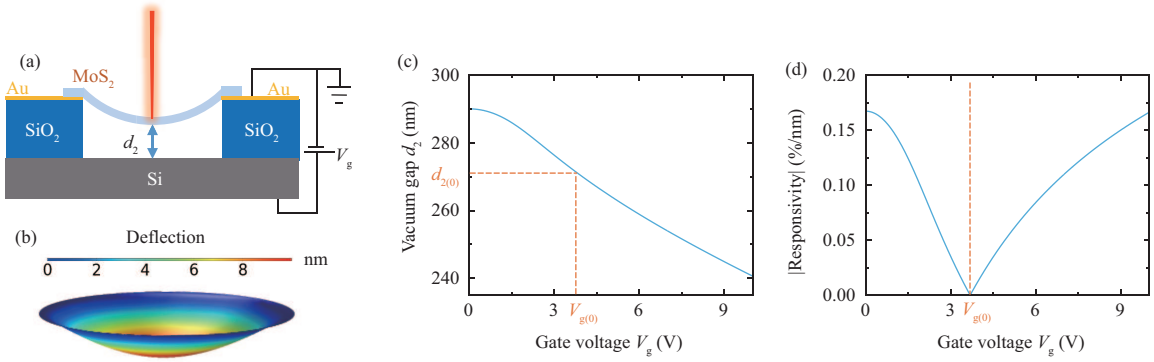

Figure 2 (Color online) Responsivity variation induced by the gate voltage. (a) Schematic illustration of a deflected MoS_2 membrane under DC gate voltage V_g. (b) Three-dimensional (3D) deflection profile of the MoS_2 membrane under V_g = 1 V, obtained through finite element simulation. (c) Analytical solution showing the vacuum gap at different V_g, using the same device parameters as in Figure 1. The vacuum gap $d_{2(0)}$ when 0 responsivity occurs corresponds to the gate voltage $V_{g(0)}$. (d) Magnitude of the interferometric responsivity as a function of V_g, clearly showing its variation before and after $V_{g(0)}$.

the responsivity. The deflection of the MoS_2 membrane under V_g can be obtained through both finite element simulations (Figure 2(b)) and analytical modeling (Figure 2(c)). Given the extremely large aspect ratio of the 2D membrane which is atomically-thin, in analytical calculation we ignore the flexural rigidity of the suspended 2D membrane, and calculate the static deflection at the center of the vacuum gap z_s (which equals the reduction in d_2) by minimizing the total energy (electrostatic energy plus elastic energy) [28], which is equivalent to setting its derivative to 0:

$$\frac{8\pi E_Y d_1}{3(1-\nu_p^2)R^2} z_s^3 + \left(\frac{2\pi E_Y d_1 \varepsilon_0}{1-\nu_p^2} - \frac{1}{2}C'' V_g^2\right) z_s - \frac{1}{2}C' V_g^2 = 0, \tag{4}$$

where E_Y is the Young's modulus of MoS_2, ν_p is the Poisson's ratio, R and d_1 are the radius and thickness of the circular membrane, C is the capacitance between the MoS_2 and the back gate, C' and C'' are the first and second derivatives of C with respect to z_s, evaluated at z_s= 0. From our calculation (using the same parameters as in Figure 1), we find that by just applying a V_g of 10 V, d_2 can decrease from 290 to 240 nm (Figure 2(c)). During this process, as the vacuum gap crosses $d_{2(0)}$, which corresponds to the gate voltage of $V_{g(0)}$, the responsivity value crosses 0, assuming the laser spot remains at the center of the membrane (Figure 2(d)). As V_g continues to increase beyond $V_{g(0)}$, the responsivity becomes nonzero again.

This finding shows that the laser interferometry responsivity can be effectively tuned by the gate voltage, and has important implications for studying 2D NEMS, as responsivity optimization plays a key role in 2D NEMS measurements, given the miniscule device size and motion amplitude. Meanwhile, in 2D device research, it is often necessary to apply a gate voltage. Therefore, understanding the effect of gate voltage on responsivity is highly important.

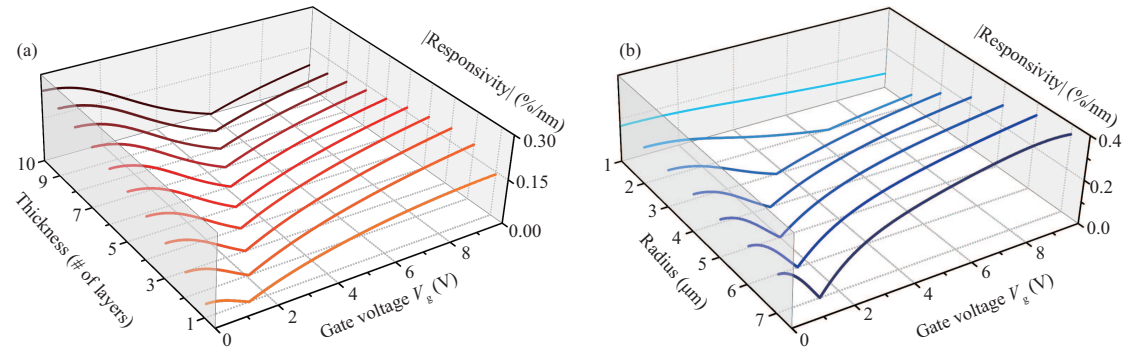

Figure 3 (Color online) Calculated responsivity at various gate voltages, for different (a) MoS_2 thicknesses (1–10 layers), and (b) MoS_2 device radius (1–7 μm).

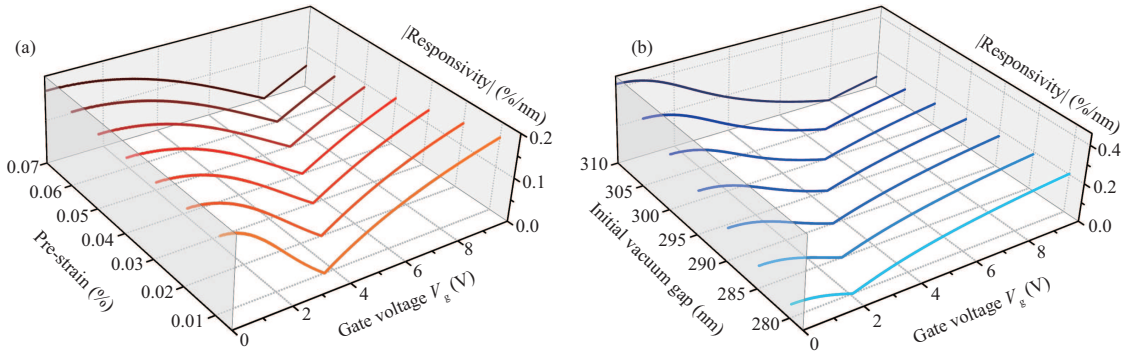

Figure 4 (Color online) Calculated responsivity at various gate voltages, for different (a) MoS_2 pre-strain values (0.01% to 0.07%), and (b) initial vacuum gap d_0 (280–310 nm).

We further analyze and quantify such effect on 2D NEMS resonators with different MoS_2 thicknesses (Figure 3(a)) and device radius (Figure 3(b)), by systematically sweeping these important device parameters in our calculations, and monitoring how the value of $V_{g(0)}$ changes in response to these parameters. In Figure 3(a), we sweep the MoS_2 thickness from 1 layer to 10 layers, while keeping the membrane radius at 3 μm. In Figure 3(b), we sweep the MoS_2 radius from 1 to 7 μm, while keeping the thickness of MoS_2 at 5 layers. We find that within the V_g range of 0 to 10 V, $V_{g(0)}$ value increases with MoS_2 thickness and decreases with device radius, consistent with the general observation that larger and thinner devices are more easily deflected towards the gate for a given gate voltage, and thus they can more easily reach the 0 responsivity configuration.

Furthermore, we analyze the 0 responsivity point for devices with different pre-strain and initial vacuum gaps (which is equal to the SiO_2 layer thickness in Figure 1(a)). Here we mainly focus on the initially-flat membrane at zero gate voltage, i.e., with initial tensile strain, which is common in suspended 2D materials. In Figure 4(a), we sweep the pre-strain in MoS_2 from 0.01% to 0.07%, which are typical values of pre-strain in 2D NEMS devices [17], and correspond to pre-tension values from 0.088 to 0.614 N/m, respectively, while keeping the initial vacuum gap $d_0 = 290$ nm. In Figure 4(b), we sweep the initial vacuum gap d_0 (the vacuum gap without applying any gate voltage) from 280 to 310 nm, while keeping the pre-strain at 0.01%. In both cases, we use $d_1 = 3.25$ nm (5 layers), and $r = 3$ μm, same as in Figure 1. We observe that the $V_{g(0)}$ value increases with pre-strain, as expected—devices with smaller pre-strain are less tight, and can be more easily deflected by the gate voltages; thus $V_{g(0)}$ occurs at smaller values. We also find that larger initial vacuum gap d_0 results in larger $V_{g(0)}$; here we note that changing the initial vacuum gap d_0 and changing the gate voltage both result in a change in d_2, so that a larger initial d_0 requires a higher gate voltage to reach the responsivity zero point. This is consistent with the results shown in Figure 1(c).

Because the $V_{g(0)}$ value depends on all these different device parameters, we summarize the collective effects of multiple such parameters on the $V_{g(0)}$ value, and present them as color maps (Figure 5). In the first case, we vary both the radius and thickness of MoS_2, and summarize the resulting $V_{g(0)}$ values in color scale in Figure 5(a). We find that thinner and larger-radius devices tend to have lower $V_{g(0)}$ values,

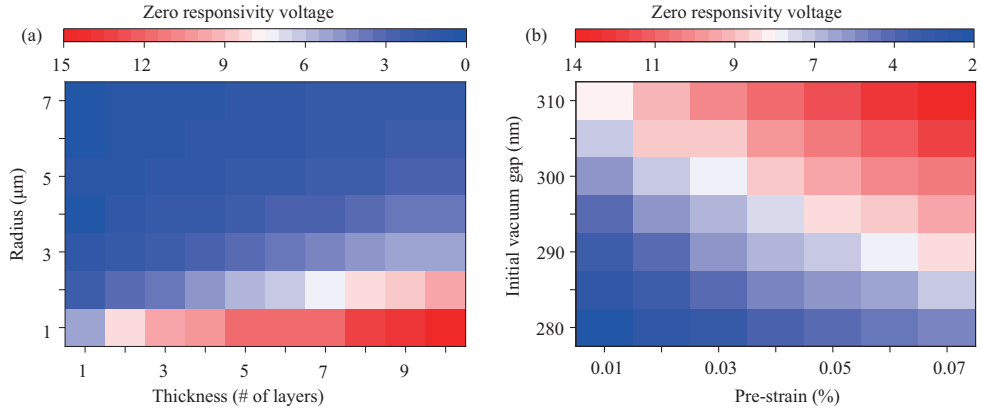

Figure 5 (Color online) Calculated $V_{g(0)}$ value in color scale, for MoS_2 NEMS resonators with different values of (a) thickness and radius (pre-strain = 0.01%, initial vacuum gap = 290 nm), and (b) pre-strain and initial vacuum gap (MoS_2 thickness = 3.25 nm, device radius = 3 μm).

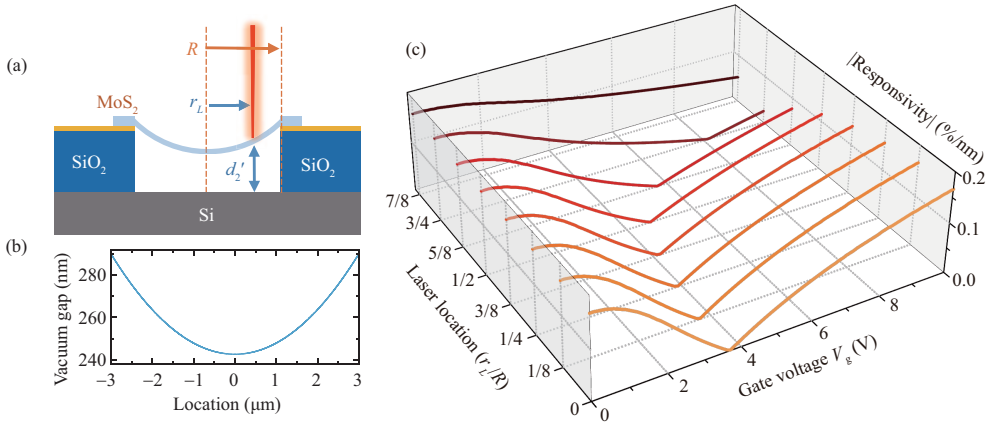

Figure 6 (Color online) Responsivity across the surface of a device with a gate-voltage-induced deflection profile. (a) Schematic illustration of an MoS_2 resonator, with the MoS_2 membrane deflected under DC gate voltage. The laser spot is positioned away from the center. The distance between the MoS_2 membrane and the bottom Si at the new laser spot position is d_2'. (b) Analytically calculated deflection profile of a 5-layer MoS_2 drumhead, with device radius of 3 μm, initial vacuum gap of 290 nm, under DC gate voltage of 10 V, and initial strain of 0.01%. (c) Magnitude of the interferometric responsivity as a function of V_g, for different laser spot positions incident on the device in (b), clearly showing how $V_g(0)$ depends on laser position.

as expected. The 2D color map can provide useful references for designing NEMS devices. For example, when measuring a given MoS_2 device, as the thickness and radius are determined, an appropriate voltage range can be chosen from the map to avoid the 0 responsivity conditions. Alternatively, for the desired voltage range, choosing the proper MoS_2 thickness and radius can help ensure sufficient responsivity throughout the measurements.

In the second case, we vary both the pre-strain and the initial vacuum gap, which are also important device parameters, so that the proper voltage range or device parameter can be properly chosen to avoid 0 responsivity conditions. Basically, for 2D NEMS resonators, their radius, thickness, initial vacuum gap, pre-strain, and applied gate voltage can all affect the responsivity, and our results presented in these multi-parameter spaces can offer useful guidelines for optimizing the measurement condition.

3 Discussion

We now analyze the position effect of gate-induced deflection of the membrane on the responsivity. In discussions above, we assume the laser spot is in the center of the membrane because when considering the fundamental flexural vibration mode, the vibration amplitude is the largest at the center, resulting in a larger detected signal for a given responsivity. When the laser spot moves away from the center position by distance r_L as shown in Figure 6(a), the different vacuum gaps at different locations will affect the interferometric responsivity. For a circularly-clamped and freely-suspended 2D membrane, the

electrostatically induced deflection profile can be approximated as $w(r) = z_s(R^2 - r^2)/R^2$, where z_s is the maximum deflection at the center (Figure 6(b)). As the laser spot position moves away from the center, the dependence of responsivity on V_g also changes, which is shown in Figure 6(c).

The results show that $V_{g(0)}$ increases with r_L, as expected. This is because further away from the center, a larger gate voltage is required to pull down the membrane to reach the same vacuum gap $d_{2(0)}$. We also find that when the laser spot is close to the center of the membrane, e.g., $r_L/R < 1/4$, the change in $V_{g(0)}$ is negligible. This suggests that a slight deviation of the laser spot position from the exact device center will not induce much change in the responsivity. Therefore, for practical purposes, our analytical results (in all other figures) remain valid by assuming the laser spot is at the device center.

4 Conclusion

In summary, we have performed a detailed analysis of electrostatic tuning of device geometry and interferometric responsivity in 2D NEMS resonators. Our results offer new insights in adjusting and optimizing signal transduction efficiency in NEMS measurements, enabling highly effective experimental exploration of device motion in these atomically-thin NEMS structures.

Acknowledgements This work was supported by the Ministry of Science and Technology of the People's Republic of China (Grant Nos. 2018YFE0115500, 2019YFE0120300), National Natural Science Foundation of China (Grant Nos. 62004026, 62004032), Science and Technology Department of Sichuan Province (Grant Nos. 2021JDTD0028, 2021YJ0517), Science and Technology Commission of Shanghai Municipality (STCSM) Natural Science Project General Program (Grant No. 21ZR1433800), and Shanghai Sailing Program (Grant No. 19YF1424900).

References

1 Kang H, Ruan B, Hao Y C, et al. Mode-localized accelerometer with ultrahigh sensitivity. Sci China Inf Sci, 2021. doi: 10.1007/s11432-020-3057-y
2 Eichler A, Moser J, Chaste J, et al. Nonlinear damping in mechanical resonators made from carbon nanotubes and graphene. Nat Nanotech, 2011, 6: 339–342
3 Jia R D, Chen L, Huang Q Q, et al. Complementary tunneling transistors based on WSe2/SnS2 van der Waals heterostructure. Sci China Inf Sci, 2020, 63: 149401
4 Xu Y F, Li W S, Fan D X, et al. A compact model for transition metal dichalcogenide field effect transistors with effects of interface traps. Sci China Inf Sci, 2021, 64: 140408
5 Morell N, Reserbat-Plantey A, Tsioutsios I, et al. High quality factor mechanical resonators based on WSe2 Monolayers. Nano Lett, 2016, 16: 5102–5108
6 Ekinci K L, Yang Y T, Roukes M L. Ultimate limits to inertial mass sensing based upon nanoelectromechanical systems. J Appl Phys, 2004, 95: 2682–2689
7 Bunch J S, van der Zande A M, Verbridge S S, et al. Electromechanical resonators from graphene sheets. Science, 2007, 315: 490–493
8 Chen C, Rosenblatt S, Bolotin K I, et al. Performance of monolayer graphene nanomechanical resonators with electrical readout. Nat Nanotech, 2009, 4: 861–867
9 Zande A M, Barton R A, Alden J S, et al. Large-scale arrays of single-layer graphene resonators. Nano Lett, 2010, 10: 4869–4873
10 Samanta C, Arora N, Vaidyuala K K, et al. The effect of strain on effective duffing nonlinearity in the CVD-MoS_2 resonator. Nanoscale, 2019, 11: 8394–8401
11 Yang R, Wang Z, Feng P X L. All-electrical readout of atomically-thin MoS_2 nanoelectromechanical resonators in the VHF band. In: Proceedings of the 29th International Conference on Micro Electro Mechanical Systems (MEMS 2016), Shanghai, 2016. 59–62
12 Yang R, Chen C, Lee J, et al. Local-gate electrical actuation, detection, and tuning of atomic-layer MoS_2 nanoelectromechanical resonators. In: Proceedings of the 30th International Conference on Micro Electro Mechanical Systems (MEMS 2017), Las Vegas, 2017. 163–166
13 Manzeli S, Dumcenco D, Marega G M, et al. Self-sensing, tunable monolayer MoS_2 nanoelectromechanical resonators. Nat Commun, 2019, 10: 4831
14 Xu Y, Chen C, Deshpande V V, et al. Radio frequency electrical transduction of graphene mechanical resonators. Appl Phys Lett, 2010, 97: 243111
15 Chen C, Lee S, Deshpande V V, et al. Graphene mechanical oscillators with tunable frequency. Nat Nanotech, 2013, 8: 923–927
16 Wang Z, Lee J, Feng P X L. Spatial mapping of multimode Brownian motions in high-frequency silicon carbide microdisk resonators. Nat Commun, 2014, 5: 5158
17 Lee J, Wang Z, He K, et al. High frequency MoS_2 nanomechanical resonators. ACS Nano, 2013, 7: 6086–6091

18 Lee J, Wang Z, He K, et al. Electrically tunable single- and few-layer MoS_2 nanoelectromechanical systems with broad dynamic range. Sci Adv, 2018, 4: eaao6653

19 Dolleman R J, Davidovikj D, van der Zant H S J, et al. Amplitude calibration of 2D mechanical resonators by nonlinear optical transduction. Appl Phys Lett, 2017, 111: 253104

20 Barton R A, Storch I R, Adiga V P, et al. Photothermal self-oscillation and laser cooling of graphene optomechanical systems. Nano Lett, 2012, 12: 4681–4686

21 Yang R, Wang Z, Wang P, et al. Two-dimensional MoS_2 nanomechanical resonators freely-suspended on microtrenches on flexible substrate. In: Proceedings of the 28th IEEE International Conference on Micro Electro Mechanical Systems (MEMS 2015), Estoril, 2015. 877–880

22 Morell N, Tepsic S, Reserbat-Plantey A, et al. Optomechanical measurement of thermal transport in two-dimensional $MoSe_2$ lattices. Nano Lett, 2019, 19: 3143–3150

23 Kim S P, Yu J, van der Zande A M. Nano-electromechanical drumhead resonators from two-dimensional material bimorphs. Nano Lett, 2018, 18: 6686–6695

24 Wang Z, Feng P X L. Interferometric motion detection in atomic layer 2D nanostructures: visualizing signal transduction efficiency and optimization pathways. Sci Rep, 2016, 6: 28923

25 de Alba R, Wallin C B, Holland G, et al. Absolute deflection measurements in a micro- and nano-electromechanical Fabry-Perot interferometry system. J Appl Phys, 2019, 126: 014502

26 Yang R, Islam A, Feng P X L. Electromechanical coupling and design considerations in single-layer MoS_2 suspended-channel transistors and resonators. Nanoscale, 2015, 7: 19921–19929

27 de Alba R, Massel F, Storch I R, et al. Tunable phonon-cavity coupling in graphene membranes. Nat Nanotech, 2016, 11: 741–746

28 Schomburg W K. Introduction to Microsystem Design. New York: Springer, 2011